Journal of Power Sources 230 (2013) 101–108

Contents lists available at SciVerse ScienceDirect

Journal of Power Sources

journal homepage: www.elsevier.com/locate/jpowsour

Review

A review on experimental evaluation of water management in a polymer electrolyte fuel cell using X-ray imaging technique

Seung-Gon Kim, Sang-Joon Lee*

Center for Bio-fluid and Bio-mimic Research, Department of Mechanical Engineering, Pohang University of Science and Technology, San 31, Hyoja Dong, Namgu, Pohang 790-784, Republic of Korea

HIGHLIGHTS

- ► X-ray imaging techniques applied to water management of PEFC are reviewed.
- ► Basic concepts of radiography and tomography are included.
- ► General developmental trend of X-ray imaging on PEFC is presented.

ARTICLE INFO

Article history:
Received 19 September 2012
Received in revised form
3 December 2012
Accepted 6 December 2012
Available online 5 January 2013

Keywords:
Polymer electrolyte fuel cell
X-ray imaging
Water management
Gas diffusion layer

ABSTRACT

Water management of polymer electrolyte fuel cell (PEFC) has been extensively studied because of its effect on the performance of a PEFC system. The transport and congelation of water significantly affect the efficiency and durability of a PEFC. Several empirical methods have been employed to visualize the spatial distribution of water in a PEFC. Experimental studies using high-resolution imaging techniques have been conducted to reveal the unknown morphological aspects that reduce the performance of a PEFC system. The X-ray imaging technique is the preferred method over other imaging techniques because of its high spatial and temporal resolution. Recently, X-ray micro computed tomography (X-ray μCT) is introduced to better characterize the anisotropic structure of a gas diffusion layer (GDL) by reconstructing its three-dimensional structure. With the development of advanced software and hardware, the X-ray imaging technique becomes essential in the visualization of water management in PEFCs. This article reviews the X-ray imaging studies on water management in a PEFC system.

1. Introduction

Polymer electrolyte fuel cell (PEFC) has recently received increasing attention as a clean renewable power source, due to its high operational efficiency and minimal environmental impact. The PEFC system is suitable for mobile applications, because its operating temperature is relatively low and its power range is appropriate for automobiles. A PEFC system consists of an electrolyte membrane, an electrode catalyst, a GDL, and a bipolar plate. The general composition of a PEFC system is shown in Fig. 1. The electrochemical reaction in a PEFC inevitably produces water, thereby dampening the electrolyte membrane [1]. The electrochemical reaction at the anode is given as:

$$H_2 \rightarrow 2H^+ + 2e^- \quad (1)$$

whereas the reaction at the cathode is:

$$\frac{1}{2}O_2 + 2H^+ + 2e^- \rightarrow H_2O \quad (2)$$

Therefore, the overall reaction in PEFC can be expressed as:

$$H_2 + \frac{1}{2}O_2 \rightarrow H_2O \quad (3)$$

Nafion® has been usually employed as electrolyte membrane for the electrochemical reaction. Nafion has proton conductivity only in the presence of water. Therefore, reactant gases supplied to the fuel cell should be humidified to ensure the efficient transport of protons. However, excessive accumulated water in the gas diffusion layer (GDL) degrades the performance and durability of PEFCs because of flooding under normal operation as well as ice formation during cold startup [2]. On the other hand, the operation with high current density and back diffusion dehydrates the anode GDL and membrane [3,4]. Both the flooding and dehydration of the membrane electrolyte assembly reduce the active area

* Corresponding author. Tel.: +82 54 279 2169; fax: +82 54 279 3199.
E-mail address: sjlee@postech.ac.kr (S.-J. Lee).

0378-7753/$ – see front matter © 2012 Elsevier B.V. All rights reserved.
http://dx.doi.org/10.1016/j.jpowsour.2012.12.030

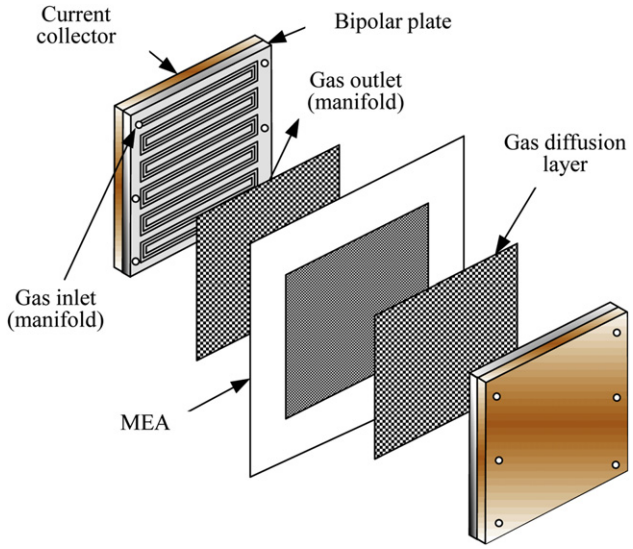

Fig. 1. Schematic diagram of a typical PEFC.

for power generation. Efficient water management is essential to maintain the performance of a PEFC. Therefore, water in a PEFC system should be analyzed precisely to understand water balance during and after operation. The water balance and removal of water from a PEFC system are key parameters that govern its efficiency and durability.

Several imaging techniques have been used to visualize the water content in a PEFC system. These methods include optical imaging [5–7], magnetic resonance imaging (MRI) [8], neutron radiography [9–13], and X-ray imaging techniques. Each imaging technique has its own advantages and disadvantages in terms of cost, material limitation, and spatial and temporal resolution. An optical imaging technique has a good temporal and spatial resolution. However, the PEFC system should have a transparent window to facilitate optical observation. Yang et al. [6] observed the generation, removal, and regeneration of water drops in the channels of a transparent unit cell with a lapse of operation time. Given that the gas channel of a PEFC is replaceable, the optical imaging technique can be applied to the water transport in the gas channels and the eruption of water droplets onto the GDL.

MRI has recently been employed to visualize the water content in PEFCs with a reasonable spatial resolution. However, this method has technological limitations in the temporal resolution and selection of composing materials of a PEFC because ferromagnetic materials distort MRI images. In 2004, Tsushima et al. [8] employed an MRI imaging technique to measure the spatial distribution of the water content in an operating PEFC. They used a special fuel cell kit made of nonmagnetic materials. The spatial and temporal resolution of the MRI is approximately 50 μm and 50 s, respectively.

Neutron radiography is highly sensitive to water. However, this method still suffers from low temporal and spatial resolution. Satija et al. [9] investigated the quantity and spatial distribution of water in a PEFC by using a neutron imaging technique. The spatial and temporal resolution of the neutron imaging system is approximately 100 μm and 1 s, respectively. Table 1 summarizes the imaging methods used to visualize water contents in a PEFC.

Most of the constituting parts of a PEFC are opaque. Therefore they require a non-invasive imaging technique for *in situ* visualization. Among the non-invasive imaging techniques, the X-ray imaging technique has high temporal and spatial resolution suitable for visualizing water transport in a PEFC. The current article will thoroughly discuss the X-ray imaging experiments to visualize the water contents and water management in a PEFC system.

2. X-ray imaging technique

2.1. X-ray radiography

X-ray imaging has been mainly used for medical and industrial applications due to its high penetration into soft tissues. A schematic diagram of an X-ray imaging system is shown in Fig. 2. As an X-ray beam transmits a test sample, variations in the thickness and composition of the internal structure produce a distinct image contrast. A scintillator crystal converts the transmitted X-ray beam into visible light that can be captured by image recording devices. When a digital camera is used to record X-ray images, the light intensity is converted into a digital signal for post-image processing. In an X-ray imaging system, the image quality is determined by an X-ray source, a scintillator, an optical relay, and a photodetector. To achieve a higher spatial resolution, a highly focused X-ray beam, a high-density scintillator, highly magnified optics, and a digital detector with small pixel size are required.

The light intensity of an X-ray beam which passes through a test sample can be expressed by the Beer–Lambert law:

$$I = I_0 e^{-\mu x} \tag{4}$$

where I is the light intensity of the X-ray beam attenuated after penetrating the test sample, I_0 is the initial non-disturbed intensity of the incident X-ray, and μ is the linear attenuation coefficient of the sample. The attenuation coefficient μ increases, as the density or atomic number (Z) of the sample increases. A material has its own inherent mass attenuation coefficient for a specific radiographic ray.

In general, water thickness in a PEFC can be obtained through the following procedure. When a test sample is composed of several constituents with different refractive indices, Eq. (4) can be generalized for a thin sample as follows:

$$I = I_0 e^{-\sum (\mu x)_i} \tag{5}$$

For an operating fuel cell composed of several different materials, Eq. (5) can be expressed as

$$I_{wet} = I_0 e^{-\left[\sum (\mu x)_{i,dry} + (\mu x)_{water}\right]} \tag{6}$$

whereas the light intensity in a dry fuel cell is expressed as:

$$I_{dry} = I_0 e^{-\left[\sum (\mu x)_{i,dry}\right]} \tag{7}$$

The amount of isolated water can be obtained by dividing the wet image (Eq. (6)) by the dry image (Eq. (7)) as follows:

$$\mu_{water} x_{water} = -\ln\left(I_{wet}/I_{dry}\right) \tag{8}$$

The thickness of the water layer (x) can be evaluated by using Eq. (8), if the linear attenuation coefficient of water (μ) is valid. However, the linear attenuation coefficient varies because of the inherent X-ray beam features of the synchrotron radiation source. Therefore, this coefficient should be evaluated based on the experimentally calibrated data. Considering that the latter PEFC image is divided by the former image during digital image processing, the resultant image contains differential information between the two images. From the divided images, the water thickness in the spot penetrated by the X-ray beam can be obtained by using Eq. (8). This image processing is called image normalization, which was first employed in the neutron imaging of the water transport in PEFCs [10].

Table 1
Advanced imaging techniques used to determine the water content in a PEFC.

Method	Spatial resolution	Temporal resolution	Advantages	Disadvantages
Optical imaging	10 μm [6]	0.06 s [6]	High spatial and temporal resolution	Transparent cell is required
MRI	50 μm [8]	50 s [8]	Sensitive to water	Incompatible with conductive materials
Neutron imaging	25 μm [13]	1 min [13]	Very high sensitive to water	Low spatial and temporal resolution
X-ray imaging	680 nm [35]	1 s [32]	High spatial and temporal resolution	Low sensitivity to water content

2.2. Synchrotron X-ray imaging technique

The synchrotron X-ray imaging technique has recently been employed to visualize the water contents in a PEFC system. The method has high spatial and temporal resolutions due to high coherency and sufficient photon flux of the synchrotron X-ray beam. A schematic diagram of a typical synchrotron X-ray imaging system is illustrated in Fig. 3. A synchrotron X-ray beam is emitted when charged particles in the storage ring are accelerated radially. When passing a double crystal monochromator (Fig. 3), the unmonochromatic X-ray beam is converted to a monochromatic beam of a single energy level. The energy level of the X-ray beam is then controlled to make the target such as water in a PEFC, suitable for capturing clear X-ray images. An X-ray photon energy of 13 keV strongly enhances the sensitivity to water [17]. The invisible X-ray images are converted into visible images after passing through a thin scintillation crystal. A high flux of synchrotron X-ray beam provides high-intensity visible light. Thus the converted X-ray images can be magnified by optical microscopic lenses. The magnified images are then captured by a digital image recording device with a high spatial resolution.

2.3. X-ray μCT

Three-dimensional (3D) tomography was used to obtain detailed information on the anisotropic structure of a GDL to understand the mass transport in a PEFC system. The mathematical basis for a tomographic imaging method was established by Radon [14]. X-ray computed tomography (CT) has been applied to obtain projected images of test samples. The projected image of a sample at a given angle Θ is composed of a set of line integrals. In X-ray CT, the line integral represents the total attenuation of the X-ray beam that transmits the sample. The intensity attenuated by the sample is given by the following equation:

$$I = I_0 e^{\left[-\int \mu(x,y)\mathrm{d}s\right]} \tag{9}$$

where $\mu(x)$ is the attenuation coefficient at a position along the ray pathway. Therefore, the total attenuation p of the X-ray at a position r, with a projection angle θ, is given by:

$$p(r,\theta) = \ln(I/I_0) = -\int \mu(x,y)\mathrm{d}s \tag{10}$$

Using the coordination system of Fig. 4, the value of r onto which point (x,y) is projected at an angle θ is given by

$$x\cos\theta + y\sin\theta = r \tag{11}$$

Therefore, Eq. (10) can be rewritten as

$$p(r,\theta) = \int_{-\infty}^{\infty}\int_{-\infty}^{\infty} f(x,y)\delta(x\cos\theta + y\sin\theta - r)\mathrm{d}x\mathrm{d}y \tag{12}$$

where $f(x,y)$ represents the attenuation coefficient $\mu(x,y)$. This function is known as the Radon transform function. Using this inverse Radon transformation, ortho-sliced images are obtained from a number of projected images.

The general procedure of X-ray μCT is demonstrated in Fig. 5. First, a large number of two-dimensional projected images are obtained consecutively by rotating the sample at a small angular interval over 180°. Next, ortho-sliced images are obtained from the projected images through the inverse Radon transformation. Finally, a 3D model is reconstructed by combining the ortho-sliced images. The 3D tomographic map of a GDL provides realistic data that can be used to validate theoretical and numerical predictions. Practical applications of X-ray imaging techniques for the visualization of water contents in a PEFC will be discussed in the following section.

3. X-ray imaging studies on water management in PEFCs

3.1. Water transport in PEFCs

In general, the term “in-plane” indicates the plane parallel to the membrane, whereas “through-plane” is the plane perpendicular to the membrane. A PEFC is assembled with multiple-layered components, such as a gas channel, GDL, catalyst layer, and membrane in the through-plane direction. Accordingly, the in-plane visualization of PEFCs is employed for water distribution and transport across the electrolyte membrane, whereas through-plane visualization is used for the transport of water in the gas channel and GDLs. To date, the water visualization of PEFC has focused on water distribution under operation, residual water after shut down, and water discharge under purging process.

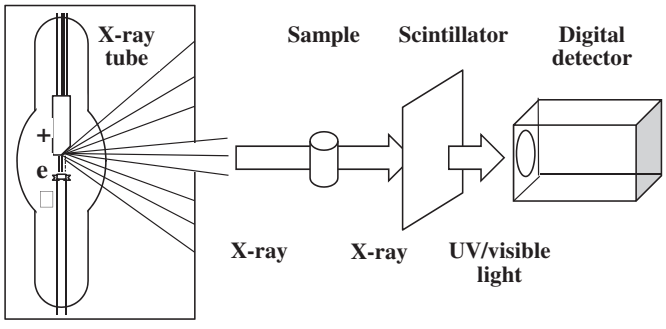

Fig. 2. Schematic diagram of an X-ray tube-based imaging technique.

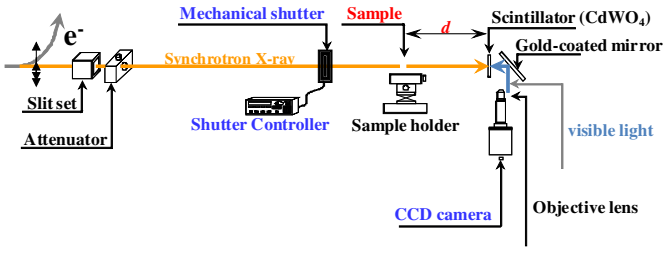

Fig. 3. Schematic diagram of synchrotron X-ray imaging system.

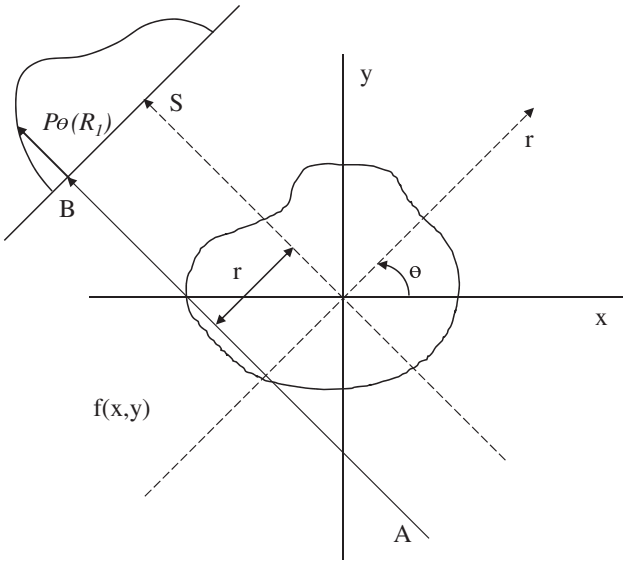

Fig. 4. Geometrical depiction of tomography.

The first PEFC study which used an X-ray beam was performed by Sinha et al. in 2006 [15]. They used an X-ray imaging technique to measure the distributions of water saturation in a GDL during a gaseous purge with a spatial resolution of 13 μm. They also employed X-ray μCT to quantify the 3D distribution of liquid water. Although its spatial resolution is still insufficient to accurately visualize the water in pores of a GDL, X-ray μCT is introduced as a powerful tool to investigate water transport in a PEFC. Manke et al. [16] employed synchrotron X-ray radiography to visualize water distribution in an operating fuel cell. The spatial resolution was approximately 3–7 μm, and the temporal resolution was approximately 4.8 s. They observed repetitive water evolution including eruptive water ejection in the fuel cell. The images of the water content in the gas channels are overlapped, because a PEFC has multiple-layered compositions in the through-plane direction. This problem was solved by using a mismatched gas channel in the anode and cathode sides.

The same research group utilized synchrotron X-ray radiography to investigate water accumulation in a GDL along the in-plane direction [17]. The experiments were conducted at the BAMline of the synchrotron BESSY in Berlin, Germany. The schematic diagram of experimental setup at BAMline is illustrated in Fig. 6. They investigated the in-plane transport of water in the GDL by using a monochromatic synchrotron X-ray imaging system with a spatial resolution of 3 μm and temporal resolution of 5 s. The water distribution in the GDL was strongly dependent on the water production related with the current density. The liquid water accumulated in the cathode GDL at high current density (420 mA cm^{-2}), and the water accumulations were observed in both anode and cathode GDLs at higher current density (600 mA cm^{-2}). The position of the diffusion barrier formation caused by the presence of water droplets was dependent on the hydrophobic or hydrophilic properties of the GDL materials.

Lee et al. [18] employed a tube-based X-ray source to test the feasibility of an X-ray imaging system to observe water accumulation in a PEFC. Typical results are shown in Fig. 7. The X-ray images of the PEFC components, such as the gas channel, rib, and GDL, are clearly distinguishable based on their different intensities. The spatial resolution of the X-ray imaging technique is sufficient to observe the water meniscus in the gas channels. In 2008, Mukaide et al. [19] observed the spatial distribution of water in an operating PEM fuel cell by using synchrotron X-ray radiography, with a spatial resolution of 12 μm and a temporal resolution of 1 s. The experiment was conducted at the BL19B2 and BL20B2 beamline of Spring-8 in Japan. Simultaneous visualization of the PEFC in the in- and through-plane directions showed that the power generation at the catalyst layer of the cathode side was inhomogeneous because of the configuration of the reactant gas inlet. They also found crack initiation resulting from increase of current density. Water filling and removal in the cracks were due to water balance between the osmotic drag and back diffusion.

Manke et al. [20] demonstrated the complementarity of the neutron imaging method and synchrotron X-ray radiography in 2009. The synchrotron X-ray they employed had a spatial resolution of 3 μm and a temporal resolution of 5 s, whereas those of the neutron imaging system were 150 μm and 10 s, respectively. The field of view for the synchrotron X-ray radiography was only 7×7 mm^2, whereas that of the neutron imaging was more than 100 mm^2, which is sufficiently large to cover the entire active area of the cells. From the experimental results obtained by both imaging techniques, the water transport and eruption of water droplets in operating PEFCs were investigated. Synchrotron X-ray radiography is suitable for visualizing the fast water transport in the GDL pores in PEFCs. In 2009, Hartnig et al. [21] investigated the liquid water formation as a function of the current density in the in-plane direction of PEFCs. The synchrotron X-ray imaging setup used in the study is similar to that in the previous one, with a spatial resolution of 3 μm and a temporal resolution of 5 s. The amount of water in the gas channels exhibited a cyclic eruption of water. The liquid water formation was mostly located beneath the rib, caused by the reduced porosity as a result of compression and the increase of electrical conductivity.

Lee et al. [22] visualized water accumulation in the cathode and anode areas of an operating PEFC. The experiment was performed at the Pohang Accelerator Laboratory (PAL) in Pohang, Korea. The spatial and temporal resolution was approximately 1 μm and 1 s, respectively. They reported that cyclic water accumulation resulted from the water balance in both GDL regions, as depicted in Fig. 8.

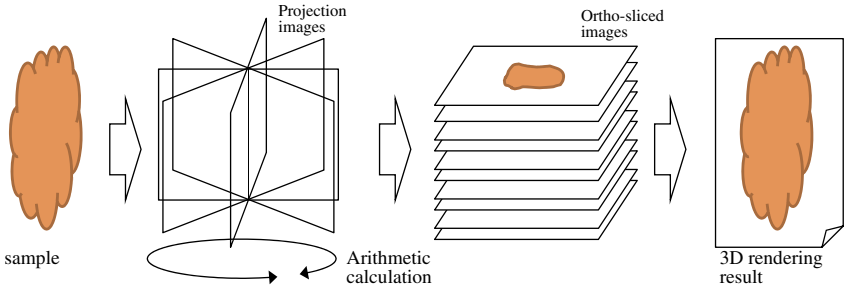

Fig. 5. Sequential procedure of X-ray CT.

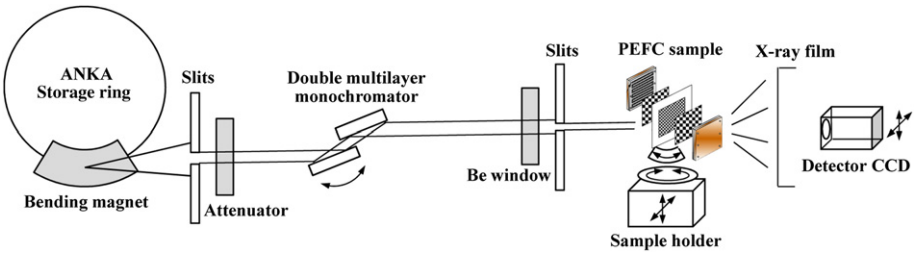

Fig. 6. Experimental setup for visualization of an operating PEFC at various current densities, as reported by Hartnig et al. [17].

The PEFC was activated when the membrane was sufficiently hydrated. Sasabe et al. [23–25] used a laboratory-based soft X-ray micro-imaging system in their visualization studies on PEFCs. The soft X-ray has photon energy of less than 2.0 keV, which is suitable for visualizing the water content in a PEFC. The spatial and temporal resolution was 1.2 μm and 2 s, respectively. In this study, the area under the rib was not effectively activated under a high current density operation (400 mA cm^{-2}). By using the soft X-ray imaging system, they investigated water accumulation along the through-plane direction [23] and the effect of morphological defects in the in-plane direction [24,25].

X-ray tomographic studies on water transport in PEFCs have been conducted under *ex situ* conditions until 2011, because of the long acquisition time needed to obtain a sufficient number of projected images to reconstruct ortho-sliced images in the tomographic analysis. More than 5 min is generally consumed to obtain projected images over 180°, with a step angle of 0.5°. Therefore, X-ray CT is hardly suitable for visualizing the rapid water transport in a PEFC system. Recently, Krüger et al. [26] demonstrated the possibility of a *quasi in situ* tomographic imaging for investigating the water distribution in PEFCs. They stopped the operation of fuel cells and sealed the gas inlet and outlet before capturing the X-ray images to prevent water movement during the experiments. By using this technique, they successfully visualized the GDL structure as well as water distribution in the PEFCs. Markötter et al. [27] adopted this *quasi in situ* tomographic technique to visualize the water distribution and 3D water transport in GDLs and adjacent micro-porous layers (MPLs).

In X-ray radiography measurements of water thickness in a PEFC, the precise determination of the X-ray attenuation coefficient μ of water is essential to the evaluation of absolute value of water thickness. X-ray attenuation is considerably dependent on the experimental setup. Thus, the calibration experiment for the attenuation coefficient μ should be performed in advance to measure water thickness accurately.

3.2. Morphological studies of PEFC components

Tomographic analysis has been commonly adopted in material science for non-invasive detection and measurement of the inner structure of a test sample. This non-invasive 3D visualization tool was mainly used to investigate the highly anisotropic structure of a GDL for better understanding of its morphological 3D structure. Becker et al. [28] compared the experimental and numerical results in terms of diffusivity, permeability, and conductivity to verify the uncertainty of the boundary condition in the numerical study of PEFCs. Both results are quantitatively consistent, except in two cases. The first mismatch occurred in the through-plane conductivity. This difference is attributed to the overestimation of the conduction from fiber to fiber. The second mismatch was the in-plane permeability caused by bias errors. This study proved that the numerical results can be used to determine the material properties of GDLs.

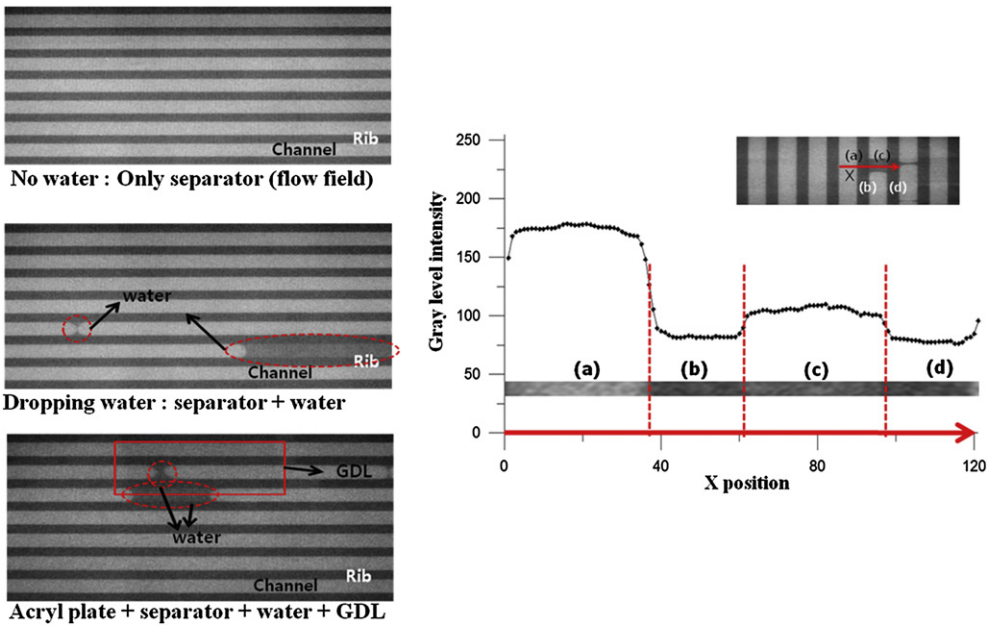

Fig. 7. Variations of gray-level intensity according to gas channel, rib and water, as reported by Lee et al. [18].

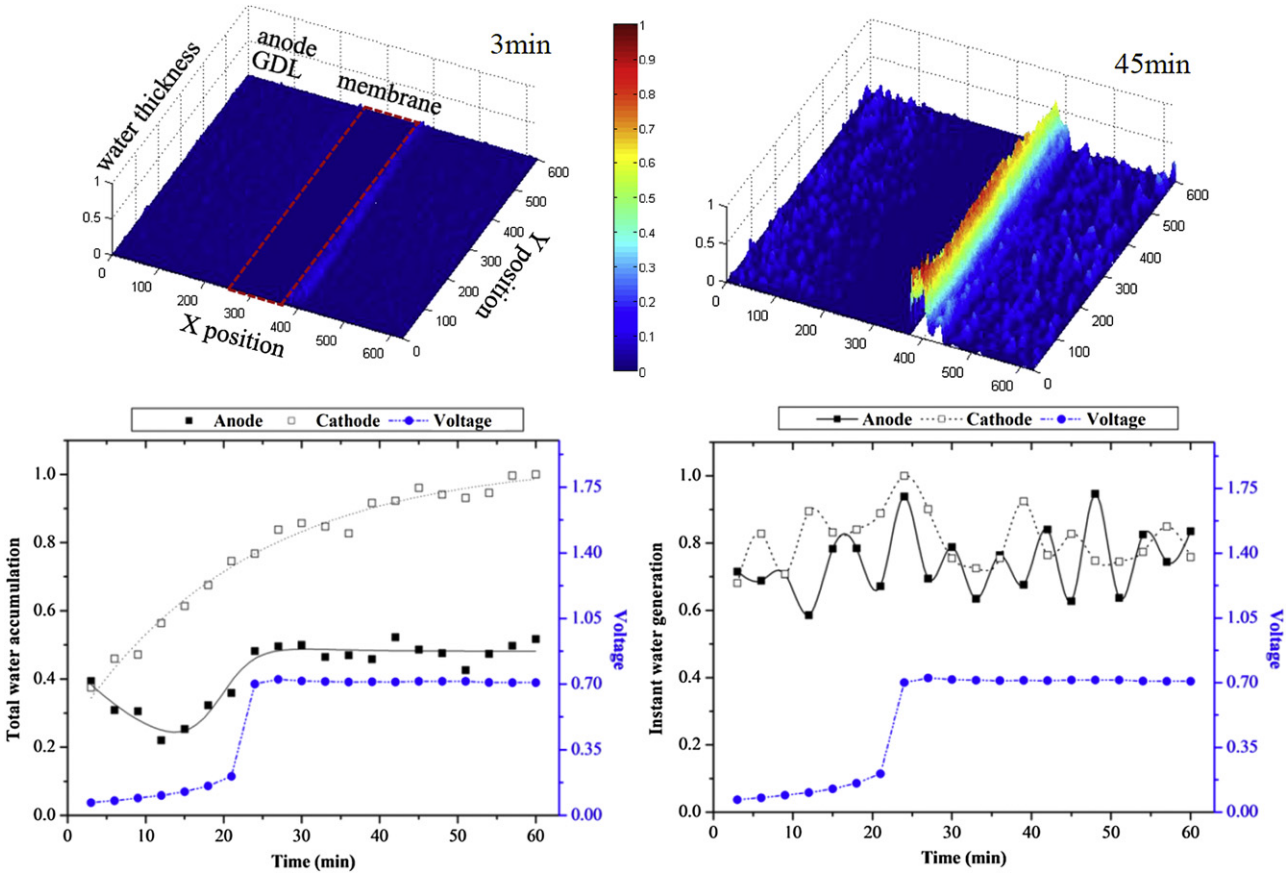

Fig. 8. Temporal variations in the water accumulation and instant water generation in the in-plane direction, as reported by Lee et al. [22].

X-ray μCT has been employed to investigate the material properties of the PEFC components. However, determining the proper threshold value for the image segmentation in tomographic analysis is difficult. Ostadi et al. [29] investigated the effect of the threshold value on determining the material properties of a GDL. They reported linear increase of porosity when the threshold value was reduced. As a result of decreased pore size, a small 3% threshold variation leads to an approximately 25% change in the Knudsen diffusion coefficient and 85% increase in permeability. Thus, they emphasized the importance of careful determination of the threshold value. Recently, Otsu's method [30] has been widely used for image segmentation [31,32]. This method automatically performs histogram shape-based image thresholding and converts a gray-level image into a binary one. The algorithm determines the optimum threshold that separates black (0 gray-level) from white (255 gray-level in an 8-bit image) to ensure that the combined intra-class variance has a minimal value.

In 2010, Pfrang et al. [33] investigated the thermal conductivity of three different types (one carbon cloth and two carbon papers) of GDL by using X-ray CT. The thermal conductivities in *x*-, *y*-, and *z*-directions were calculated by using the energy equation. However, carbon fibers and PTFE are not distinguished clearly in the CT results. Therefore, accurate discrimination remains a challenge. After the X-ray CT was found to be feasible, it has been employed by several research groups to measure the material properties of the PEFC components [34,35].

In 2010, Ostadi et al. [36] employed a desktop nano-tomography of 680 nm spatial resolution and a dual-beam FIB/SEM system with 14 nm resolution for 3D reconstruction of a GDL and an MPL, respectively. They calculated the variation in the effective diffusivity as a function of pore saturation from the experimental data. The average pore sizes in the GDL and MPL were approximately 15 μm and 137 nm, respectively. Based on the experimental results, the tortuous flow paths were numerically simulated by using the Lattice Boltzman method.

The morphological defects in the PEFC components were detected by using a high-resolution X-ray CT. The defects including cracks and holes contribute to the water transport paths and water accumulation zones [31,37,38].

In the study of material properties, the through-plane porosity distribution is a key parameter because the main flow of reactant gases and liquid water flow occurs along the through-plane direction. Fishman and Bazylak [39–41] reported a series of heterogeneous porosity distribution in the through-plane using X-ray CT. The same research group conducted related studies for tortuosity, effective diffusivity, and permeability [39], as well as the effects of PTFE [40] and MPL cracks [41]. These studies on the heterogeneous porosity distribution provide new perspectives in the analysis of the material properties of GDLs.

Recently, tomographic analysis was performed in the study of GDLs under an artificially controlled environment. Kim and Lee [38] and Je et al. [42] reported the morphological variations of GDLs under freeze-thaw cycles. Both experiments were conducted in the 7B2 beamline of PAL in Pohang, Korea, with approximately 1 μm spatial resolution. Both research groups explained the effect of freeze-thaw cycles on the output of a PEFC system. The typical reconstructed images of a GDL which adhere to the MPL layer are illustrated in Fig. 9. By using the synchrotron X-ray CT, Kim and Lee [38] visualized an opaque GDL with a highly anisotropic structure and protruding fibers, as shown in Figs. 9(b) and (c). The protruding

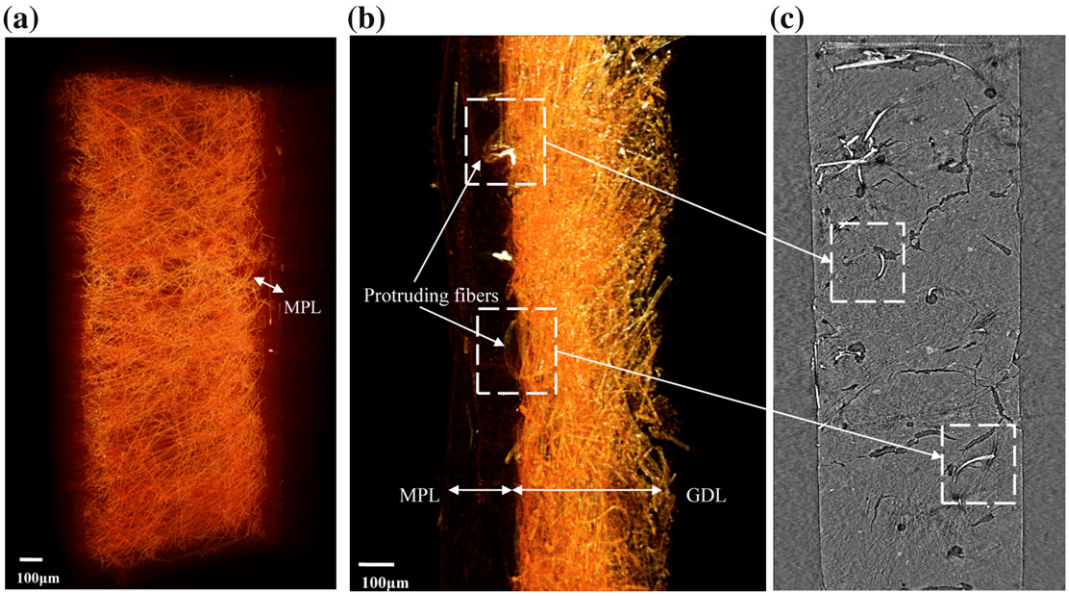

Fig. 9. Reconstructed image of a GDL adhered to an MPL, as demonstrated by Kim and Lee [38].

fibers contribute to crack initiation in the MPL region. In 2012, Kim et al. [43] investigated the variations in water pressure with respect to the breakthrough and drainage pressures by using synchrotron X-ray CT. These studies largely contributed to the understanding of water transport in GDLs under various environmental conditions.

In the studies using X-ray tomography, the post-image processing, acquisition time for X-ray images, and time for 3D reconstruction are key issues that should be addressed. The threshold value affects the evaluation of material properties significantly. Thus, the thresholding technique needs to be improved. The phase-contrast imaging technique [28,44], which uses coherent synchrotron X-ray beam, can efficiently identify solid and void regions of the PEFC components. Moreover, given that X-ray images inevitably contain noises caused by the X-ray beam fluctuations and optical distortions, appropriate filtering procedures should be considered for noise reduction. The time for image acquisition and reconstruction of X-ray μCT should be largely reduced for *in situ* analysis of water management in an operating PEFC.

4. Summary

The X-ray imaging technique has been employed to study the water transport in a PEFC. It has been successfully applied to visualize the water content and morphological structure of a PEFC system. X-ray radiography is suitable for studying the water management in a PEFC because it has a higher spatial and temporal resolution compared to other imaging techniques. X-ray μCT provides details of water transport in a GDL by adopting a tomographic technique over conventional radiography. The general developmental trend of X-ray imaging techniques is summarized in Table 2. X-ray imaging techniques still have several technological limitations, such as low sensitivity to water and long acquisition time for capturing images in X-ray CT. However, advances in X-ray imaging techniques can better explain water management of PEFC systems by resolving the current technological issues. Conclusively, the innovative X-ray imaging technique is essential to improve the performance of PEFCs.

Table 2
Advances in the X-ray imaging technique employed in the PEFC study.

Year	2006–2009	2009–2012
PEFC operation	*ex situ*	*in situ* (*quasi in situ*)
Dimension	2-dimensional radiography	3-dimensional tomography
Resolution	Tens of μm/few seconds	Few μm/under 1 s
Target	Flow field in gas channel	Mass transport in anisotropic GDL

Acknowledgements

This work was supported by the Creative Research Initiatives (Diagnosis of Biofluid Flow Phenomena and Biomimetics Research) of MOST/NRF of Korea.

References

[1] F. Barbir, PEM Fuel Cell: Theory and Practice, Elsevier Academic Press, 2005.
[2] M. Mench, Fuel Cell Engines, John Wiley & Sons, 2008.
[3] T.E. Springer, T.A. Zawodzinski Jr., S. Gottesfeld, J. Electrochem. Soc. 138 (1991) 2334.
[4] T. Okada, G. Xie, M. Meeg, Electrochem. Acta 43 (1998) 2141.
[5] K. Tüber, D. Pócza, C. Hebling, J. Power Sources 124 (2003) 403.
[6] X.G. Yang, F.Y. Zhang, A.L. Lubawy, C.Y. Wang, Electrochem. Solid State Lett. 7 (11) (2004) A408.
[7] K. Nishida, T. Murakami, S. Tsushima, S. Hirai, J. Power Sources 195 (2010) 3365.
[8] S. Tsushima, K. Teranish, S. Hirai, Electrochem. Solid State Lett. 7 (9) (2004) A269.
[9] R. Satija, D.L. Jacobson, M. Arif, S.A. Werner, J. Power Sources 129 (2004) 238.
[10] T.A. Trabold, J.P. Owejan, D.L. Jacobson, M. Arif, P.R. Huffman, Int. J. Heat Mass Transf. 49 (2006) 4712.
[11] J.P. Owejan, T.A. Trabold, D.L. Jacobson, D.R. Baker, D.S. Hussey, M. Arif, Int. J. Heat Mass Transf. 49 (2006) 4721.
[12] A. Turhan, K. Heller, J.S. Brenizer, M.M. Mench, J. Power Sources 160 (2006) 1195.
[13] P. Boillat, D. Kramer, B.C. Seyfang, G. Frei, E. Lehmann, G.G. Scherer, A. Wokaun, Y. Ichikawa, Y. Tasaki, K. Shinohara, Electrochem. Commun. 10 (2008) 546.
[14] J.H. Radon, Ber vor Sächs Akad Wiss 69 (1917) 262.
[15] P. Sinha, P. Halleck, C.Y. Wang, Electrochem. Solid State Lett. 9 (7) (2006) A244.
[16] I. Manke, C. Hartnig, M. Grünerbel, W. Lehnert, K. Kardjilov, A. Haibel, A. Hilger, J. Banhart, Appl. Phys. Lett. 90 (2007) 174105.
[17] C. Hartnig, I. Manke, R. Kuhn, N. Kardjilov, J. Banhart, W. Lehnert, Appl. Phys. Lett. 92 (2008) 134106.
[18] S.J. Lee, N.Y. Lim, S. Kim, G.G. Park, C.S. Kim, J. Power Sources 185 (2008) 867.
[19] T. Mukaide, S. Mogi, J. Yamamoto, A. Morita, S. Koji, K. Takada, K. Uesugi, K. Kajiwara, T. Noma, J. Synchrotron Radiat. 15 (2008) 329.
[20] I. Manke, C. Hartnig, N. Kardjilov, H. Riesemeier, J. Goebbels, R. Kuhn, P. Kruger, J. Banhart, Fuel Cells 10 (1) (2010) 26.
[21] C. Hartnig, I. Manke, R. Kuhn, S. Kleinau, J. Goebbels, J. Banhart, J. Power Sources 188 (2009) 468.
[22] S.J. Lee, S.G. Kim, G.G. Park, C.S. Kim, Int. J. Hydrogen Energy 35 (2010) 10457.

[23] T. Sasabe, S. Tsushima, S. Hirai, Int. J. Hydrogen Energy 35 (2010) 11119.
[24] T. Sasabe, P. Deevanhxay, S. Tsushima, S. Hirai, Electrochem. Commun. 13 (2011) 638.
[25] T. Sasabe, P. Deevanhxay, S. Tsushima, S. Hirai, J. Power Sources 196 (2011) 8197.
[26] Ph Krüger, H. Markötter, J. Haußmann, M. Klages, T. Arlt, J. Banhart, Ch. Hartnig, I. Manke, J. Scholta, J. Power Sources 196 (2011) 5250.
[27] H. Markotter, I. Manke, Ph. Kruger, T. Arlt, J. Haussmann, M. Klages, H. Riesemeier, C. Hartnig, J. Scholta, J. Banhart, Electrochem. Commun. 13 (2011) 1001.
[28] J. Becker, R. Fluckiger, M. Reum, F. Buchi, F. Marone, M. Stampanoni, J. Electrochem. Soc. 156 (2009) B1175.
[29] H. Ostadi, P. Rama, Y. Liu, R. Chen, X.X. Zhang, K. Jiang, Chem. Eng. Sci. 65 (2010) 2213.
[30] N. Otsu, IEEE Trans. Sys. Man Cyber. 9 (1) (1979) 62.
[31] Z. Fishman, J. Hinebaugh, A. Bazylak, J. Electrochem. Soc. 157 (11) (2010) B1643.
[32] S.G. Kim, S.J. Lee, Int. J. Hydrogen Energy 37 (2011) 566.
[33] A. Pfrang, D. Veyret, G. Janssen, G. Tsotridis, J. Power Sources 196 (2011) 5272.
[34] S. Takeya, A. Yoneyama, J. Miyamoto, Y. Gotoh, K. Ueda, K. Hyodo, T. Takeda, J. Synchrotron Radiat. 17 (2010) 813.
[35] H. Ostadi, P. Rama, Y. Liu, R. Chen, X. Zhang, K. Jiang, Microelectron. Eng. 87 (2010) 1640.
[36] H. Ostadi, P. Rama, Y. Liu, R. Chen, X. Zhang, K. Jiang, J. Membr. Sci. 351 (2010) 69.
[37] A. Pfrang, D. Veyret, F. Sieker, G. Tsotridis, Int. J. Hydrogen Energy 35 (2010) 3751.
[38] S.G. Kim, S.J. Lee, Int. J. Hydrogen Energy 37 (2012) 566.
[39] Z. Fishman, A. Bazylak, J. Electrochem. Soc. 158 (2) (2011) B247.
[40] Z. Fishman, A. Bazylak, J. Electrochem. Soc. 158 (8) (2011) B841.
[41] Z. Fishman, A. Bazylak, J. Electrochem. Soc. 158 (8) (2011) B846.
[42] J.H. Je, J.R. Kim, M. Kaviany, S.Y. Son, M.H. Kim, J. Synchrotron Radiat. 18 (2011) 743.
[43] J.R. Kim, J.H. Je, T.J. Kim, M. Kaviany, S.Y. Son, M.H. Kim, Curr. Appl. Phys. 12 (2012) 105.
[44] P. Cloetens, M. Pateyron-Salomè, J.Y. Buffière, G. Peix, J. Baruchel, F. Peyrin, M. Schlenker, J. Appl. Phys. 81 (9) (1997) 5878.